# Electric Propulsion Mission Life Prediction using a Multi-Fidelity Modeling Framework

# IEPC-2025-585

Presented at the 39th International Electric Propulsion Conference, Imperial College London, London,
United Kingdom
14-19 September 2025

Christopher M. Cretel, and Richard E. Wirz<sup>†</sup>
Oregon State University, Corvallis, Oregon, 97331, United States

We present and analyze results from a gridded ion thruster predictive engineering model (GIT PEM). The GIT PEM integrates coupled models of ion optics, erosion, electron back-streaming, and facility effects, reformulated for fast simulation times, enabling statistically significant ensembles for mission life uncertainty analysis. Validation against the NASA Solar Technology Application Readiness thruster long duration (LDT) and extended life (ELT) tests demonstrates good agreement with observed trends. Compared to state-of-the-art ion optics codes such as CEX2D, the GIT PEM produces similar results but reduces computational time from hours to seconds, enabling rapid assessment of thruster behavior. By explicitly accounting for facility effects in closed-system vacuum chamber tests, the model improves representation of in-space operation and erosion processes. Results show that competing facility effects can mask true erosion and backstreaming behavior; if not properly understood, these effects may lead to overestimation of thruster lifetime.

### I. Introduction

The NASA funded Joint AdvaNced PropUlsion InStitute (JANUS) was established to proliferate high power electric propulsion (EP) systems through experimental and computational efforts. High power EP exacerbates thruster interactions with the facility that have shown to alter thruster performance even in lower power systems. To study facility effects and quantify the mission uncertainty associated with extrapolating ground test data to space, JANUS has developed the predictive engineering model (PEM) framework. The PEM aims to assess high power thruster life and performance and to provide quantifiable uncertainty to life-limiting phenomena and mission analysis. This framework couples thruster, environment, and power electronics models to provide a systems level analysis in a way that is computationally tractable.

There are many ongoing efforts in electric propulsion research to model and measure facility effects. For instance, varying types of optical emission spectroscopy (OES) have been deployed to non-intrusively gather data from the thruster plume. Spatial OES provides a wide-field perspective of the plume and using specific wavelength filters, the relative neutral and ion densities can be observed.<sup>5</sup> FastOES has been deployed to resolve oscillations in the cathode plume typically accredited to the predator-prey phenomena.<sup>6,7</sup> Additionally, new models of neutral transport are being developed to more accurately capture the interactions neutral particles have with complex vacuum chamber geometry and how particle incident angles affect flux back to the thruster face.<sup>8</sup>

High-fidelity ion optics models capture ion trajectories, collisions, erosion, and electron backstreaming, 9, 10 but are too computationally expensive for the large ensembles needed in uncertainty quantification. CEX2D-tebs, for example, iteratively solves the Poisson equation and propagates ions until convergence. Even simple cases require minutes to run, while simulations with significant erosion and backstreaming can take hours, meaning Monte Carlo studies with thousands of samples would span months to years. Such runtimes are impractical for design, ensemble-based uncertainty quantification, or real-time control.

 $<sup>^\</sup>dagger \textsc{Executive}$  Director, Aerospace Research Programs, richard.wirz@oregonstate.edu



<sup>\*</sup>PhD Student, Mechanical/Aerospace Engineering, cretelc@oregonstate.edu

The GIT PEM supports JANUS' charge of enabling uncertainty quantification by reducing the computational complexity while maintaining similar generality to CEX2D. The GIT PEM utilizes many of same mathematical models as CEX2D while incorporating additional models to study facility effects. Charge exchange ion generation, electron backstreaming current, and CEX impingement erosion are all examples of mathematical models that the GIT PEM shares with CEX2D. In addition, the GIT PEM has incorporated a parsimonious carbon backsputtering sputtering model to account for the masking of and reduction in the erosion rate as a result of carbon deposition on the grids. The objective of the GIT PEM, therefore, is to maintain the model fidelity of high-fidelity ion optics models while significantly reducing computation time. By meeting this objective, we are enabling statistically significant ensembles of simulations that can be used in quantifying mission uncertainty.

# II. Model Description

Gridded ion thrusters represent one of the most widely employed electric propulsion architectures. In these systems, a discharge chamber produces a dense plasma upstream of a pair of carefully aligned perforated grids. The grid in direct contact with the plasma, known as the *screen grid*, maintains the discharge plasma at an elevated potential. Downstream, the *accel grid*, biased to a negative potential relative to the discharge chamber, extracts and accelerates ions into the plume. Collectively, the screen and accelerates ion prices assembly, a critical determinant of thruster performance and lifetime.

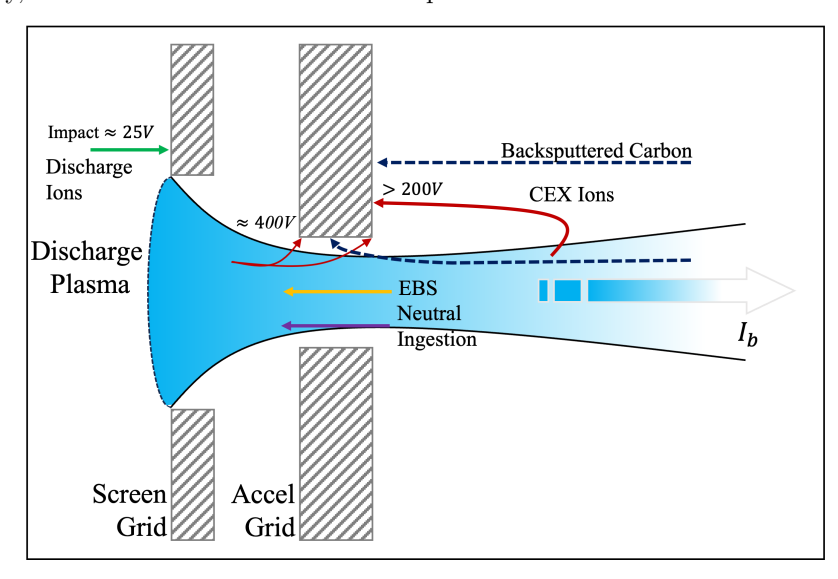


Figure 1: Several particle transport mechanisms occur simultaneously within the gridlet of an ion thruster. CEX and discharge ions cause erosion of the accel and screen grids, carbon deposits mask erosion of the screen grid, and neutral ingestion changes the discharge plasma parameters. Electron backstream constitutes the metric by which we assess the life of the gridded ion thruster.

A schematic of a single aperture pair, or "gridlet", is provided in Figure 1, along with several additional relevant processes for the GIT-PEM. To first order, grid erosion drives gridded ion thruster life. Erosion arises from the interplay of two competing processes: charge exchange (CEX) ion impingement and carbon deposition. CEX ions are produced both within the ion optics and in the near-plume region, where a significant density of neutrals escaping the discharge chamber is present. As ions are accelerated, collisions with neutrals result in CEX and/or momentum exchange (MEX) interactions. Post-collision ions possess significantly reduced momentum and are therefore more readily influenced by the electric fields around the accel grid. As they are accelerated by the grid's electric field the CEX ions acquire sufficient energy to sputter material from the grid surfaces, thereby eroding the grid geometry. Simultaneously, plume ions strike facility surfaces and sputter material that subsequently redeposits onto the grids. Many vacuum chambers are lined with graphite, so the sputtered material typically carbon. The redeposited carbon replaces sputtered grid material, decreasing the net erosion rate. The mitigating effect is enhanced by the relatively low sputter yield of carbon compared with molybdenum, the conventional grid material.



At the plasma–screen grid interface, a sheath forms to balance ion and electron fluxes. Following Bohm's classical sheath criterion, a negative potential proportional to the plasma temperature draws ions toward the surface while repelling electrons, thereby preserving quasi-neutrality.<sup>12</sup> Although the energy imparted to sheath-entering ions is small relative to that of CEX ions, the ion flux incident on the screen grid surface is significantly larger, making sheath-driven erosion as substantial of a contributor to grid wear as CEX impingement on the accel grid.

Another important failure mode is electron backstreaming, in which high-energy electrons traverse the accel grid potential barrier and enter the discharge chamber. This phenomenon, observed in the NSTAR thrusters, represents the primary life-limiting mechanism.<sup>11</sup> Backstreaming electrons increase the power load on the power processing unit (PPU) without providing commensurate thrust, thereby reducing system efficiency. As accel grids erode, the applied potential must be raised to preserve electron suppression. Once the required potential exceeds the PPU limit, uncontrolled electron backstreaming occurs and the thruster's operating range must be constrained.

#### A. Erosion

Grid erosion is the result of frequent particle bombardment on the grids and the mechanism that leads to gridded ion thrusters failure. During ground testing, carbon deposition competes with erosion and slows the observed erosion rates by replacing sputtered material and decreasing sputter yield. Equation 1 represents the sputtered flux from CEX ion impingement including both singly and double charged ions. <sup>10</sup> Additionally, the carbon surface coverage,  $\theta_C$  has been included to capture the carbon backsputter effects. <sup>13</sup> We would like to note that in following the equations, we define  $\Gamma$  as the flux incident on the computational surface area. Accordingly, the equations reduce to units of particles/s. When implemented in the code for a prescribed area, however, the units remain consistent with flux, i.e., particles/sm<sup>2</sup>.

$$\Gamma_{CEX}^{s} = \Gamma_{CEX}^{C} \frac{1 - \theta_{C}}{1 - \gamma} \left[ Y(\varepsilon_{CEX}^{+}) + Y(\varepsilon_{CEX}^{++}) \frac{\gamma}{2} \frac{\sigma_{CEX}^{++}(\varepsilon_{++})}{\sigma_{CEX}^{+}(\varepsilon_{+})} \right]$$
(1)

 $\Gamma^{C}_{CEX}$  is the flux of ions generated from CEX collisions.  $Y(\varepsilon^{+/++}_{CEX})$  is the yield of sputtered material per the Eckstein sputter model using Yim's parameters. The CEX collision cross section,  $\sigma(\varepsilon_{+/++})$  are calculated via Miller's model ( $\sigma = A - Blog(\varepsilon)$ ). The input variables,  $\varepsilon_{+/++}$  and  $\varepsilon^{+/++}_{CEX}$  represent the relative kinetic energy of an incident ion with a target neutral and the acquired kinetic energy of a CEX ion as it impinges on the surface of the grid, respectively. The inclusion of (+) and (++) as subscripts and superscripts indicates the charge of the incident ion.

Equation 2 describes the CEX ions generation by a beam of ions through a density of neutral particles  $(n_0)$  within some volume (V).<sup>17</sup>

$$\Gamma_{CEX}^{C} = \frac{j}{q} n_0 \sigma_{CEX}^{+}(\varepsilon) V \tag{2}$$

Equation 2 is uniquely determined by the geometric parameter of interest; accel radius  $(r_a)$  and accel thickness  $(t_a)$ . The primary source of CEX ions that erode the grid aperture are assumed to originate from the area between the grids where the neutral density is essentially the local neutral density in the discharge chamber. For the accel grid thickness erosion, these CEX ions are born from collision with facility neutrals, therefore the local facility neutral density is used.

The screen grid is eroded by ions accelerating through the discharge plasma sheath. Equation 3 is the double-ion-corrected sputter flux from sheath ions. $^{4,10}$ 

$$\Gamma_{dis}^{s} = \frac{1}{1+\gamma} \Gamma_{Bohm} \left[ Y(\varepsilon^{+}) + \frac{\gamma}{2} Y(\varepsilon^{++}) \right]$$
(3)

The flux of sputtered material from the grids translates to an erosion rate dependent on the grid's mass density  $(\phi_{grid})$  and atomic mass  $(\bar{M})$ .

$$\dot{x} = \Gamma_{CEX}^{S,x} \frac{\bar{M}_{grid}}{N_A \rho_{grid}} \tag{4}$$

The grid geometry is updated by the simple forward Euler method via Equation 5.

$$x(t) = \dot{x}_{t-1}\Delta t + x_{t-1} \tag{5}$$



This process is repeated for  $x = r_a$ ,  $t_a$  and  $t_s$  at each timestep.

## 1. Carbon Deposition

$$\theta_C = \frac{\Gamma_C}{\Gamma_{CEX}^C Y_{C-Mo}} \tag{6}$$

Carbon surface coverage is given by Eq. 6.<sup>13,18</sup>  $\Gamma_C$  is the flux of carbon deposition,  $\Gamma^C_{CEX}$  is the flux of CEX ions impinging on the accel grid (Equation 2), and  $Y_{C-Mo}$  is the Xe-Mo sputter yield modified by the presence of a single layer of carbon deposited on a molybdenum grid. Soulas<sup>18</sup> calculates  $Y_{C-Mo} \approx 0.99$  which is used in the analysis herein.

The GIT PEM models sputtered carbon atoms as a 1D flux of carbon back to the thruster as a result of plume ion impingement on a carbon-based beam target, given by Equation 7.

$$\Gamma_C = \frac{Y_C I_B}{q} \frac{A_{th}}{A_{ch}} \tag{7}$$

 $Y_C$  is the sputter yield of incident ions on carbon,  $I_B$  is the total ion beam current,  $A_{th}$  and  $A_{ch}$  are the surface areas of the thruster face and the area over which the plume impinges on the thruster respectively.  $A_{ch}$  is determined from the plume divergence half-angle,  $\theta_{plume}$  and the thruster distance to the wall,  $L_{wall}$ .

### B. Electron Backstreaming

Grid erosion weakens the potential barrier retarding electrons from streaming back into the thruster. Electrons with sufficient energy to overcome the potential barrier and traverse into the discharge chamber are called backstreaming electrons. The current of backstreaming electrons is determined by integrating over accel grid aperture along the local minimum radial potential profile,  $\phi_m(r)$ .

$$I_{ebs} = 2\pi \left(\frac{en_{bp}\bar{c}}{4}\right) \int_{0}^{r_{max}} exp\left[\frac{\phi_{m}(r) - \phi_{bp}}{T_{e}}\right] dr$$
 (8)

In Eq. 8,  $n_{bp}$ ,  $T_e$  and  $\phi_{bp}$  are plasma density, electron temperature and plasma potential of the beam plasma, respectively. The parameter  $\bar{c} = \sqrt{8eT_e/\pi m_e}$  is the thermal velocity of the neutralizing electrons.

The potential profile,  $\phi_m$ , is not explicitly known in Equation 8 without numerically solving Poisson's equation which leads to long simulation run times. The objective of the GIT PEM is to be fast, therefore we avoid numerical solutions. Past CEX2D simulations and the study of a large dataset of potential fields in the region  $r = [0, r_a]$  shows that the potential can be approximated by a simple second order polynomial  $(\phi_m(r) \approx ar^2 + br + c)$ .<sup>19</sup> A second order polynomial has 3 coefficients which are determined from the 3 boundary conditions for  $\phi_m(r)$ ;  $\phi_m(r=0) = \phi_{sp}$ ,  $\phi_m(r=r_a) = V_a$  and  $\frac{d\phi_m}{dr}|_{r=0} = 0$ . Applying these conditions, the coefficients are found to be  $a = (V_a - \phi_{sp})/r_a^2$ , b = 0, and  $c = \phi_{sp}$ , thus the potential profile is approximated by Equation 9.

$$\phi_m(r) \approx \frac{V_a - \phi_{sp}}{r_a^2} r^2 + \phi_{sp} \tag{9}$$

The integral is solvable when Eq. 9 is plugged into Eq. 8. Equation 10 is the result of performing the integration from 0 to  $r_a$ 

$$I_{ebs} = \frac{\pi r_a^2 e T_e}{V_a - \phi_{sp}} \left( \frac{n_{bp} \bar{c}}{4} \right) \exp \left[ \frac{\phi_{sp} - \phi_{bp}}{T_e} \right] \left( \exp \left[ \frac{V_a - \phi_{sp}}{T_e} \right] - 1 \right)$$
(10)

 $V_{ebs}$  is the voltage applied to the accel grid  $(V_a)$  such that the electron backstreaming current  $I_{ebs}$  is held below some predetermined threshold. Typically, this is expressed as a fraction of the beam current  $R_{ebs} = I_{ebs}/I_B$  or beamlet current,  $R_{ebs} = I_{ebs}/I_b$  where  $R_{ebs} = 0.1$  when using  $I_B$  and  $R_{ebs} = 0.01$  when using  $I_b$  on the centerline. Because  $V_{ebs}$  is only weakly dependent on the parameter  $R_{ebs}$  over several orders of magnitude, we have chosen  $R_{ebs} = 0.01$  because the focus of the simulation is on a single gridlet rather than the entire



grid system. We specify a new dimensionless variable and combine the remaining constants.

$$\Phi = \frac{V_a - \phi_{sp}}{T_e}$$

$$c_1 = \pi r_a^2 e \left(\frac{n_{bp}\bar{c}}{4}\right)$$

$$c_2 = \exp\left[\frac{\phi_{sp} - \phi_{bp}}{T_e}\right]$$
(11)

A more tractable form of Eq. 10 can now be written.

$$R_{ebs}I_B = c_1c_2 \frac{\exp\Phi - 1}{\Phi} \tag{12}$$

Eq.12 cannot be solved analytically for  $\Phi$ , but the equation may be simplified by analyzing the terms that make up  $\Phi$ . With  $V_a \approx -10^3$ ,  $\phi_{sp} \approx 10^1$  and  $T_e = \mathcal{O}(1)$ , then  $\Phi \approx -10^3$ . Since  $\exp \Phi \ll 1$  the exponential expression in Eq. 12 can be neglected, enabling an analytic solution without loss of accuracy.

$$R_{ebs}I_B = \frac{-c_1c_2}{\Phi} \to \Phi = \frac{-c_1c_2}{R_{ebs}I_B}$$
 (13)

The saddle point potential  $(\phi_{sp})$  is the last remaining unknown to be found, but Williams et al.<sup>20</sup> derived an expression for  $\phi_{sp}$  that can be used.

$$\phi_{sp} = \phi_{bp} + T_e \ln \left( 2R_{ebs} \sqrt{\phi \left( \frac{m_e}{M} \right) \left( \frac{\phi_{dp} - \phi_{bp}}{T_e} \right)} \right)$$
 (14)

Up to now, the space-charge effect of the beamlet has been ignored, however the potential profile may be sensitive to this modification, especially for high power systems where the beam current density may be high. Fortunately, Williams et al. have also derived a simple analytical expression for the beamlet space-charge effect.

$$\Delta \phi = \frac{j_b}{2\pi\varepsilon_0} \sqrt{\frac{M}{2e(\phi_{dp} - \phi_{sp})}} \left[ \frac{1}{2} - \ln\left(\frac{d_b}{d_a}\right) \right]$$
 (15)

Finally, solving Equation 13 for  $V_a$  and applying the space charge modification from Eq. 15 we can determine  $V_{ebs}$ .

$$V_{ebs} = \phi_{sp} + \Delta\phi - \frac{c_1 c_2 T_e}{R_{ebs} I_B} \tag{16}$$

We have now determined analytical equations for grid erosion,  $r_a$ ,  $t_a$ , and  $t_s$  and coupled those to the metric determining thruster life,  $V_{ebs}$ . The following section describes how the coupling of these equations corresponds to empirical data from the NSTAR LDT and ELT test campaigns, demonstrates the model's ability to translate ground test data to a space-like environment, and finally an example use case it assess mission life uncertainty.

## III. Results & Discussion

# A. Model Set Up

The extensively documented NSTAR thruster provides a robust dataset for validating the GIT PEM. We compare against two major test campaigns: the Long Duration Test (LDT), which operated an engineering model thruster (EMT) at 2.3 kW (TH15) for 8,200 hours, and the Extended Life Test (ELT). During the LDT, electron backstreaming voltage,  $V_{ebs}$ , was measured at multiple power levels, and post-test aperture diameters were recorded for comparison.<sup>21</sup>

The ELT campaign operated the Deep Space 1 flight spare thruster for over 32,000 hours in a 3 m diameter by 10 m long chamber. It was specifically noted that the chamber was lined with graphite panels to mitigate sputtering. Power was varied by alternating between TH15 and lower throttle conditions in



 $\tilde{5},000$ -hour intervals, as summarized in Table 1. Throughout the test,  $V_{ebs}$  was recorded regularly, with additional off-centerline data and beam current density profiles at several throttle settings.  $^{9,11}$ 

Table 1: Transposed NSTAR Throttle Table 10

Test Segment [khrs]	0 – 0.5	0.5 – 4.75	4.75 - 10.5	10.5 – 15.6	15.6 - 21.3	21.3 – 25.75	25.75 - 32
Throttle Level	TH 12	TH 15	TH 8	TH 15	TH 0	TH 15	TH 5

The GIT PEM requires tuning parameters (Table 2), which are either difficult to measure or simplify in the reduced-order model. For example, the average kinetic energy of CEX ions ( $E_{CEX}$ ) is approximated. Likewise, the fraction of CEX ions in the plume that impinge on the grids rather than the facility is captured in the correction factor  $\eta_p$ . Similarly, local grid erosion is approximated by a control variable  $\eta_{b1}$  to distribute erosion between downstream and upstream  $(1-\eta_{b1})$  accel grid vertices, with  $\eta_{b1}=.75$  approximating observed chamfer erosion. These parameters represent *epistemic* uncertainties, reducible with additional data.

Table 2: Model tuning parameters

Symbol	Value	Unit	Description	Distribution
$\eta_p$	see Distribution	-	cex ion impingement probability in the plume	$\mathcal{U}(0.001, 0.01)$
$\eta_{b1}$	see Distribution	-	upstream cex ion impingement probability between the grids	$\mathcal{U}(0.5, 0.85)$
$R_{ m ebs}$	0.001	-	electron backstreaming ratio limit	-
w	0.5		weight of upstream accel vertex used in $r_{a,avg}$ calculation	-
$E_{\text{cex}}$	see Distribution	$\mathrm{eV}$	charge-exchange collision energy	$\mathcal{U}(300, 500)$

Table 3 lists the thruster parameters used in the GIT PEM, which include grid material and geometry, selected plume conditions, and propellant type. The LDT and ELT campaigns used the EMT and FMT, which differ in accel grid thickness,  $(t_a)$ . Most parameters are well understood or constrained by fabrication tolerances, but plume quantities  $(\phi_{plume})$  are more uncertain. Grid separation  $(l_g)$  is also particularly influential<sup>22</sup> and experiments have shown it can vary in time,<sup>23</sup> creating significant uncertainty in its true operating value.

The vacuum facility parameters (Table 4) represent our knowledge of the operating environment. By careful adjustment of these parameters, the GIT PEM can emulate either a vacuum test facility or space (i.e  $n_{0,fac} \approx 6 \times 10^{14}~m^{-3}$  and  $L_{wall} = \infty$ ).<sup>24</sup> Facility neutral density  $(n_{0,fac})$  is highly non-uniform in vacuum chambers thus uncertainty is introduced depending on pressure gauge and vacuum pump placement.<sup>8</sup> Thruster-to-wall distance  $(L_{wall})$  is likely understood to within  $\pm 1~cm$ . The representative uncertainty is greater than the actual uncertainty to account for non-standard chamber wall geometry.

Table 5 lists the throttle conditions used in the GIT PEM. Uncertainties in these inputs are represented with *Normal* distributions for parameters that can take negative values and *LogNormal* for strictly positive values. Among them, discharge and near-plume plasma parameters are the primary divers of uncertainty, directly influencing screen and accel grid erosion and electron backstreaming.

To quantify uncertainty, the GIT PEM takes N=1000 samples of the uncertainty values, propagates these inputs in a Monte Carlo scheme and produces time-dependent distributions of key outputs. Erosion introduces dynamic behavior in thruster operation, thus the output distribution parameters additionally evolve over time. The following results validate the GIT PEM against LDT and ELT data and then demonstrate how facility interactions shape mission life predictions.

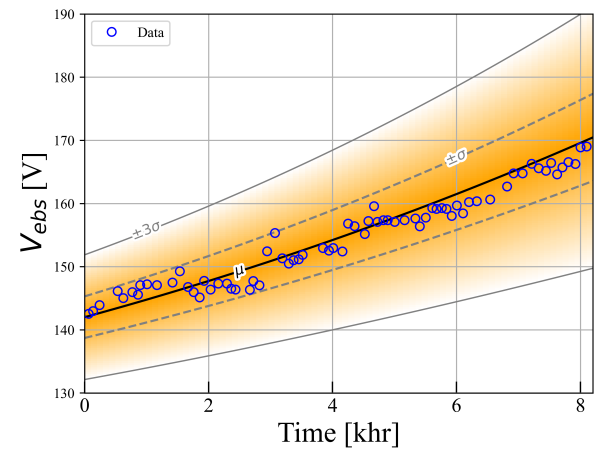
## B. Results

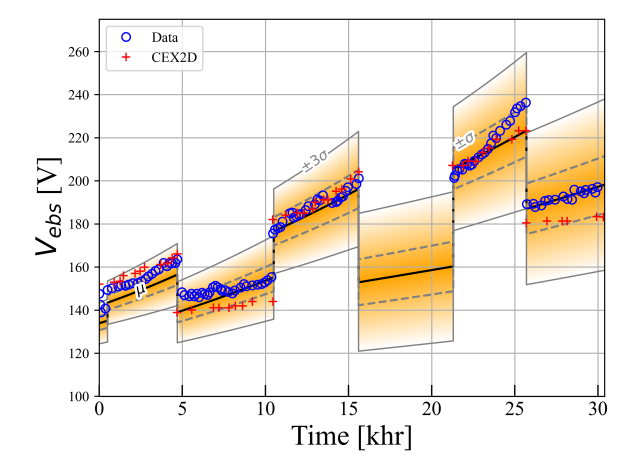
The LDT  $V_{ebs}$  data provides a good starting dataset to validate the GIT PEM. In Figure 2a we compare the GIT PEM output with measured ground test data from the LDT. The data falls well within the output uncertainty of our model, shown by the light blue around the nominal value. The general trend of increasing



Table 3: NSTAR EMT and FMT parameters

Symbol	Value	Unit	Description	Distribution
$R_t$	0.15	m	thruster major radius	-
$\theta$	20	$\deg$	plume divergence half angle	-
$\phi_{ m bp}$	13	V	plume potential	$\mathcal{N}(\cdot,20\%)$
$T_{e,\mathrm{bp}}$	1.35	${ m eV}$	plume electron temperature	$\log \mathcal{N}(\cdot, 25\%)$
$N_i$	54		propellant atomic number	-
$M_i$	134.27	g/mol	propellant atomic mass	-
$l_g$	0.36	mm	grid separation	$\log \mathcal{N}(\cdot, 10\%)$
$r_s$	0.955	mm	screen grid radius	-
$r_{a,u}$	0.57	mm	accel grid radius (discharge side)	-
$r_{a,d}$	0.57	mm	accel grid radius (vacuum side)	-
s	2.24	mm	aperture center spacing	-
$t_a$	EMT: 0.51 FMT: 0.38	mm	accel grid thickness	-
$t_s$	0.38	$_{ m mm}$	screen grid thickness	-
$M_g$	95.95	g/mol	grid material atomic mass	-
$ ho_g$	0.01022	$\rm g/mm^3$	grid material density	-
$N_{ m ap}$	13000	-	nominal number of apertures (est.)	-





(a) Measured  $V_{ebs}$  data for the LDT overlaid on GIT PEM predictions, with model mean  $(\mu)$  and confidence bounds shown. The data align closely with the model within the  $\pm \sigma$  bounds.

(b) Experimental  $V_{ebs}$  data from the ELT and CEX2D results compared with GIT PEM predictions. The PEM captures the observed behavior across test segments, with most measurements contained within the  $\pm\sigma$  bounds.

Figure 2: The GIT PEM is validated on LDT (a) and ELT (b) data. Uncertainty bounds are the result of running the GIT PEM N=1000 times, each time picking at random samples from the input probability distribution functions listed in Tables 2-5.

 $|V_{ebs}|$  (note that  $V_{ebs} < 0$ ) of the empirical data is also captured by the GIT PEM. The spread of the empirical data points obfuscates higher order trends such as whether the trends is accelerating, decelerating or linear, whereas the GIT PEM suggests that this trend could be accelerating slightly. This would have significant ramifications to predicting mission life from this data set, which will be discussed later in this section. While the LDT data represents a simple data set to validate our model, the objective of the GIT PEM is to simulate actual missions which typically require the thruster to throttle power. To follow up on



Table 4: Environmental/Facility parameters

Symbol	Value	Unit	Description	Distribution
$n_{0,\mathrm{fac}}$	$2.0\times10^{18}$	$\mathrm{m}^{-3}$	facility neutral density	$\log \mathcal{N}(\cdot, 25\%)$
$n_{0,\mathrm{space}}$	$6.0\times10^{15}$	$\mathrm{m}^{-3}$	space neutral density	$\log \mathcal{N}(\cdot, 25\%)$
$R_{ m ch}$	3	$\mathbf{m}$	cylindrical vacuum chamber radius	-
$L_{ m ch}$	10	$\mathbf{m}$	cylindrical vacuum chamber length	-
$N_s$	6	-	vacuum chamber wall material atomic number	-
$M_s$	12.011	g/mol	vacuum chamber wall material atomic mass	-
$ ho_C$	$2.25{\times}10^6$	$g/m^3$	redeposited material density	-
$L_{\mathrm{wall}}$	5	m	downstream distance from thruster to wall	$\log \mathcal{N}(\cdot, 5\%)$

Table 5: Throttle Conditions

Sym.	TH0	TH5	TH8	TH12	TH15	Unit	Description	Distribution
$I_B$	0.51	0.81	1.10	1.49	1.76	A	total beam current	-
$I_b$	1.0e-4	1.7e-4	2.1e-4	2.45e-4	2.7e-4	A	beamlet current	-
$V_T$	650	850	1100	1100	1100	V	total (discharge) potential	-
$V_a$	-150	-150	-180	-180	-180	V	applied accel grid potential	-
$\phi_{dp}$	20.0	25.5	26.5	26.0	32.0	V	discharge plasma potential	$\mathcal{N}(\cdot, 10\%)$
$n_{bp}$	2.10e17	$2.45\mathrm{e}17$	2.80 e17	$3.15\mathrm{e}17$	3.50 e17	$\mathrm{m}^{-3}$	near-field plume ion density	$\log \mathcal{N}(\cdot, 20\%)$
$n_{dp}$	$1.00 \mathrm{e} 17$	$1.00 \mathrm{e} 17$	$1.00 \mathrm{e} 17$	1.00 e17	1.50 e17	$\mathrm{m}^{-3}$	discharge ion density	$\log \mathcal{N}(\cdot, 20\%)$
$n_{n,dp}$	1.50 e18	1.50 e18	1.50 e18	1.50 e18	1.50e18	$\mathrm{m}^{-3}$	discharge neutral density	-
$T_{e,dp}$	6.0	6.0	6.0	6.0	6.0	$\mathrm{eV}$	discharge electron temperature	$\log \mathcal{N}(\cdot, 15\%)$
$\gamma$	0.04	0.125	0.14	0.175	0.15		double-single ion current ratio	-

the LDT data validation, we include the ELT data validation which demonstrates the GIT PEMS ability to resolve multiple throttle conditions.

Similar to Figure 2a, Figure 2b compares the GIT PEM to empirical ELT data. Additionally, CEX2D simulations were available and are overlaid on the GIT PEM output as well. The same model inputs were used here as in the LDT GIT PEM simulation, with the exception of throttle-specific parameters. As expected, the additional complexity of changing throttle conditions leads to wider uncertainty in the GIT PEM output and, during some test segments, a divergence from the measured data. However, the general trends and accuracy are encouragingly accurate, replicating the accuracy of the output from CEX2D quite well over the entire simulated campaign. The fifth test segment (21.3-25.75 khrs), neither CEX2D nor GIT PEM are able to accurately replicate the increased slope of the  $|V_{ebs}|$  data. One hypothesis is the GIT PEM's treatment of the potential profile, which is agnostic to the accel grid thickness. It is expected that the potential profile that results from thinning of the accel grid due to plume CEX erosion would be weaker than what is currently simulated in the GIT PEM; this change could capture the measured trends. However, CEX2D, which does resolve the potential profile as the accel grid thins, also does not capture this trend. Even so, except for Test Segment 1, the measured data and CEX2D simulation results fall within the predicted model uncertainty throughout the simulated campaign.

The validation of the GIT PEM demonstrates that much of the accuracy associated with high fidelity models, like CEX2D, was not lost during the order-reduction that produced the GIT PEM. This is encouraging, because it provides a platform by which statistically significant ensembles of simulations can be produced with quantifiable uncertainties. In the rest of the section, this capability is presented by demonstrating how mission life may be affected by facility effect and what effect this has on mission life uncertainty.

The key to ground testing lies in the ability of the data to represent a space-like environment. Figure 3 shows the results of the GIT PEM when simulating a space-like environment. Overlaid on the graph



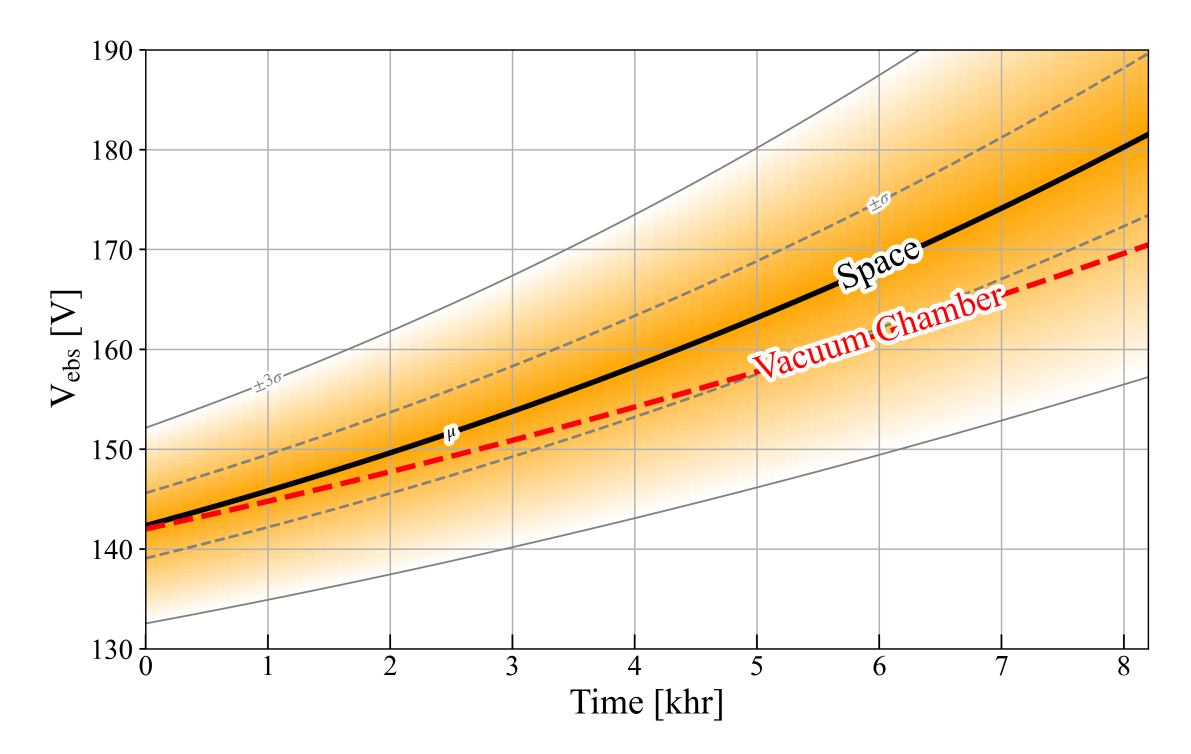


Figure 3: Eliminating facility effects (e.g.,  $n_{0,fac} = 6 \times 10^{15}$ ,  $L_{wall} = \infty$ ) increases the predicted  $V_{ebs}$ , demonstrating that neglecting carbon backsputter can result in underestimation of mission life metrics.

is the result shown in Figure 2a where the environment was a finite volume vacuum chamber. The same model inputs were used to generate both plots, however the environmental parameters,  $n_{0,fac} \to n_{0,space}$  and  $L_{wall} \to \infty$  are adjusted appropriately such that CEX ion generation is reduced in the plume and carbon backsputter is non-existent. It should be noted that  $n_{0,space} \neq 0$  because there is a finite particle density even in low earth orbit as well as a flux of neutrals escaping from the discharge chamber through the grids.

For the first 5 khrs, the expected  $V_{ebs}$  during vacuum chamber operation remains within one standard deviation of the corresponding in-space prediction. Over the full simulated campaign, both ground and space cases remain within three standard deviations of each other; however, the in-space condition consistently predicts higher  $|V_{ebs}|$  than ground testing. This indicates that the reduction in carbon backsputter from ground to space is not balanced by the corresponding change in CEX ion generation and erosion. By distinguishing carbon deposition from CEX-driven erosion, the GIT PEM facilitates the translation of ground test data to in-space operation. These results have important implications for the design of vacuum chambers and for the community's ability to apply ground test data to mission analysis. Further exploration of chamber design space with high-fidelity models is warranted to verify these findings; nonetheless, the results indicate that mitigating carbon deposition to the thruster will improve agreement between ground and space environments.

Table 6: Simulated Mission Profile

Test Segment [khrs]	0 - 10	10 – 50
Throttle Level	TH 15	TH 8

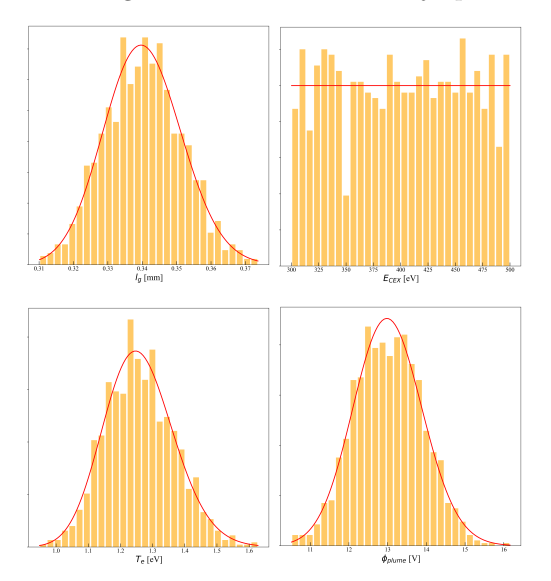
The objective of the GIT PEM is to assess mission life uncertainty. Figure 4 illustrates this capability by simulating a mission-like profile and quantifying the associated uncertainty in mission duration. Table 6 lists the set points and test segment durations used. The values  $n_{0,space}$  and  $L_{wall} = \infty$  are used. The left-side panels show example input distributions for four representative parameters, selected from the broader set of uncertainty inputs to the GIT PEM. Propagation of these inputs yields the  $V_{ebs}$  evolution shown on the right. The red dashed line denotes the NSTAR power processing unit (PPU) voltage limit,  $V_{th} = 300 \text{ V}$ , which defines the operational constraint on throttle conditions. Figure 4 thus characterizes the uncertainty



in the time at which  $|V_{ebs}|$  first exceeds  $V_{th}$ . In the ELT campaign, during the third TH15 test segment,  $V_{ebs}$  exceeded the voltage rating on the power supplies, thus restricting thruster operation to set points below TH15.<sup>11</sup> In the present model realization, the thruster is *expected* to remain fully operational for approximately 29 khrs. However, by 20 khrs there is a growing probability that  $V_{ebs}$  will surpass  $V_{th}$ , thus requiring a reduction in throttle set point.

An artifact of the growing uncertainty in  $V_{ebs}$  is the apparent reversal of the  $-3\sigma$  trend line. This behavior is considered non-physical, as no mechanisms exist in space that would reverse grid erosion, which the trend would otherwise imply. Ongoing application of the GIT PEM will focus on determining whether this feature arises from unresolved physical processes or from limitations in the current treatment of input uncertainties, which can be refined as improved data become available.

Finding that there is a probability the thruster may fail or that its operating range could be reduced sooner than expected is important because it directly links model predictions to mission risk. Quantifying this probability allows engineers to anticipate when operational constraints (like  $V_{ebs} > V_{th}$ ) may occur, enabling proactive design adjustments, contingency planning, and improved mission assurance. Without this insight, thruster performance and lifetime estimates from ground testing are potentially misleading, obscuring critical risks that could jeopardize mission objectives.



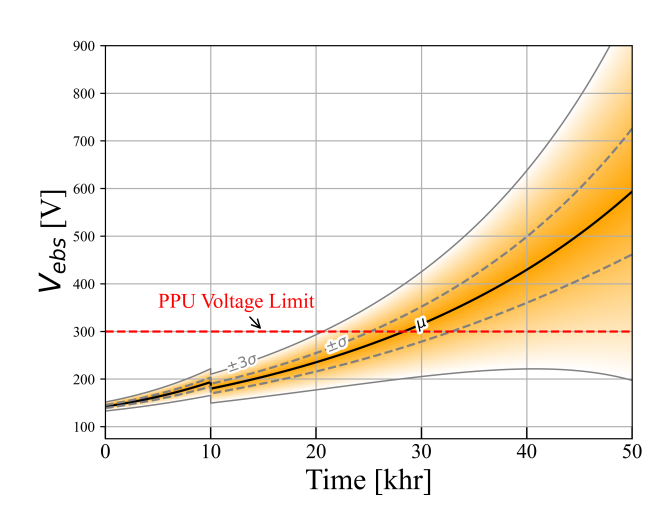


Figure 4: Representative input distributions (left) and resulting  $V_{ebs}$  evolution from the GIT PEM (right). The red dashed line denotes the NSTAR PPU voltage limit ( $V_{th} = 300 \text{ V}$ ). The model expects full throttle capability to  $\sim 29 \text{ khrs}$ , but with finite probability of exceeding  $V_{th}$  by 20 khrs.

While the GIT PEM has demonstrated generally accurate representation of the LDT and ELT campaigns, the lack of existing neutral and sputterant transport models remains a key area of improvement. Fortunately, there are ongoing efforts within the JANUS organization to develop these models which will be incorporated in the future. The GIT PEM still uses semi-empirically derived models for the potential sub-model which limits its full predictive capabilities. The GIT PEM simulates 1000s of samples in seconds, therefore it may be beneficial to reintroduce higher-fidelity computational schemes that are capable of resolving the potential field as well as a global model of the discharge chamber to incorporate neutral ingestion effects on the discharge plasma. To accommodate the latter, facility ingestion flux would be introduced as a new facility parameter.

# IV. Conclusion

The GIT PEM has been developed to enable statistical analysis of mission life metrics, with validation against NSTAR ELT and LDT campaign data demonstrating strong agreement across a wide range of operating conditions and mission profiles. Implementation of a carbon deposition model distinguishes between erosion behavior in finite-sized vacuum chambers and space environments, thus allowing the GIT PEM to translate performance from ground test data. Overall, the GIT PEM achieves similar results to the higher-



fidelity CEX2D code while considerably reducing computational time from hours to seconds. Because of this time-savings, there may be an appetite to re-introduce higher-fidelity models where appropriate or explore more advanced data-driven techniques to remove reliance on the tuning parameters in Table 2. However, these next steps must not degrade the GIT PEM's ability to run large-scale Monte Carlo simulations.

The GIT PEM uses straight forward statistical methods to quantify the output uncertainty from input probability distributions. However, more sophisticated methods exist and have been incorporated in other models.<sup>25–27</sup> The GIT PEM only differentiated aleatoric and epistemic uncertainties via the distribution functions. The use of Sobol index analysis and Bayesian inference are ways in which we can improve our knowledge of the input distributions and ultimately quantify the input sensitivities to guide future experimental efforts toward better understanding of those parameters.

# Acknowledgments

We want to thank our funding from the Joint Advanced Propulsion Institute (NASA Grant No. 80NSSC21K1118) and Dr. Justin Koo's Propulsion and Power Program at the Air Force Office of Scientific Research (AFOSR Award No. FA9550-25-1-0012)

#### References

- <sup>1</sup>M. L. Walker, D. Lev, M. Saeedifard, B. Jorns, J. Foster, A. D. Gallimore, A. Gorodetsky, J. L. Rovey, H. B. Chew, D. Levin, *et al.*, "Overview of the joint advanced propulsion institute (janus)," in *37th International Electric Propulsion Conference*, 2022.
- <sup>2</sup>J. E. Foster and T. J. Topham, "A review of the impact of ground test-related facility effects on gridded ion thruster operation and performance," *Physics of Plasmas*, vol. 31, p. 030501, Mar. 2024.
- <sup>3</sup>T. Topham, Understanding the Mechanisms Affecting Gridded Ion Engine Operation in Ground Test Facilities. PhD thesis, University of Michigan, 2025.
- <sup>4</sup>R. E. Wirz, A. Gorodetsky, B. Jorns, and M. L. R. Walker, "Predictive Engineering Model for Life and Performance Assessment of High-Power Electric Propulsion Systems," p. 20, June 2022.
- <sup>5</sup>I. J. Hofbeck and R. E. Wirz, "Spatial spectroscopy for hall thruster plume species," in *Proceedings of the International Electric Propulsion Conference (IEPC)*, (London, UK), 2025. (IEPC-25-630).
- <sup>6</sup>M. F. Konopliv, L. K. Johnson, and R. E. Wirz, "Time-resolved electron temperature oscillations in hall thrusters," *Journal of Applied Physics*, vol. 137, no. 24, 2025.
- <sup>7</sup>A. M. Harteloo and R. E. Wirz, "Broadband characterization of hall thruster discharge and cathode multimode plasma oscillations via fastoes," in *Proceedings of the International Electric Propulsion Conference (IEPC)*, (London, UK), 2025. (IEPC-25-665).
- <sup>8</sup>R. A. Obenchain and R. E. Wirz in *Proceedings of the International Electric Propulsion Conference (IEPC)*, (London, UK), 2025. (IEPC-25-606).
- <sup>9</sup>R. E. Wirz, I. Katz, D. M. Goebel, and J. R. Anderson, "Electron backstreaming determination for ion thrusters," *Journal of Propulsion and Power*, vol. 27, no. 1, pp. 206–210, 2011. Publisher: American Institute of Aeronautics and Astronautics Inc.
- <sup>10</sup>R. E. Wirz, J. R. Anderson, and I. Katz, "Time-dependent erosion of ion optics," *Journal of Propulsion and Power*, vol. 27, no. 1, pp. 211–217, 2011. Publisher: American Institute of Aeronautics and Astronautics Inc.
- <sup>11</sup>A. Sengupta, J. Brophy, and K. Goodfellow, "Status of the Extended Life Test of the Deep Space 1 Flight Spare Ion Engine After 30,000 Hours of Operation," in 39th AIAA/ASME/SAE/ASEE Joint Propulsion Conference and Exhibit, (Huntsville, Alabama), American Institute of Aeronautics and Astronautics, July 2003.
- <sup>12</sup>D. Bohm, Characteristics of Electrical Discharges in Magnetic Fields, ch. 3, pp. 77–86. New York: McGraw-Hill Book Company, 1948.
- <sup>13</sup>J. E. Polk, O. Duchemin, C.-S. Ho, and B. Koel, "The Effect of Carbon Deposition on Accelerator Grid Wear Rates in Ion Engine Ground Testing."
- <sup>14</sup>W. Eckstein and R. Preuss, "New fit formulae for the sputtering yield," *Journal of Nuclear Materials*, vol. 320, no. 3, pp. 209–213, 2003.
- <sup>15</sup>J. T. Yim, "A survey of xenon ion sputter yield data and fits relevant to electric propulsion spacecraft integration," in 35th International Electric Propulsion Conference, Oct. 2017.
- <sup>16</sup>J. S. Miller, S. H. Pullins, D. J. Levandier, Y.-h. Chiu, and R. A. Dressler, "Xenon charge exchange cross sections for electrostatic thruster models," *Journal of Applied Physics*, vol. 91, pp. 984–991, Feb. 2002.
- <sup>17</sup>R. Wirz, "Long duration assessment of electron backstreaming for ion optics.," in *Proc. of the 31st Int. Electric Propulsion Conf.*, (Michigan), Sept. 2009.
- <sup>18</sup>G. C. Soulas, "The Impact of Back-Sputtered Carbon on the Accelerator Grid Wear Rates of the NEXT and NSTAR Ion Thrusters," in 33rd International Electric Propulsion Conference, (Washington DC, USA), 2013.
- <sup>19</sup>C. M. Cretel and R. E. Wirz, "Ion thruster grid life and performance assessment via reduced order modeling," in 38th International Electric Propulsion Conference, (Toulouse, France), June 2024.
- <sup>20</sup>G. D. Williams, John and P. Wilbur, "Analytical Model of Electron Backstreaming for Ion Thrusters," in 39th AIAA Joint Propulsion Conference, (Huntsville, Alabama), AIAA, July 2003.



- <sup>21</sup>J. Polk, J. Anderson, J. Brophy, V. Rawlin, M. Patterson, J. Sovey, and J. Hamley, "An overview of the results from an 8200 hour wear test of the NSTAR ion thruster," in 35th Joint Propulsion Conference and Exhibit, (Los Angeles, CA, U.S.A.), American Institute of Aeronautics and Astronautics, June 1999.
  - <sup>22</sup>R. Wirz, "Coupled analysis of ion thruster grid erosion and electron backstreaming," Space Propulsion, 2010.
- <sup>23</sup>E. M. Diaz and G. C. Soulas, "Grid gap measurement for an nstar ion thruster," in 29th International Electric Propulsion Conference, no. NASA/TM-2006-214249, 2006.
- <sup>24</sup>P. Crandall and R. E. Wirz, "Air-breathing electric propulsion: mission characterization and design analysis," *Journal of Electric Propulsion*, vol. 1, no. 1, p. 12, 2022.
- <sup>25</sup>B. A. Jorns, A. Gorodetsky, I. Lasky, A. Kimber, P. Dahl, B. S. Peter, and R. Dressler, "Uncertainty Quantification of Electrospray Thruster Array Lifetime," in *36th International Electric Propulsion Conference*, (Vienna, Austria), 2019.
- <sup>26</sup>S. Parmar, A. Collins, and R. E. Wirz, "A Bayesian Data-driven Model for Quantifying Electrospray Lifetime," in 37th International Electric Propulsion Conference, (Cambridge, Mass), 2022.
- <sup>27</sup>J. D. Eckels, T. A. Marks, M. G. Allen, B. A. Jorns, and A. A. Gorodetsky, "Hall thruster model improvement by multidisciplinary uncertainty quantification," *Journal of Electric Propulsion*, vol. 3, no. 1, p. 19, 2024.

